Competing states in a Couette-Taylor system with an axial flow

Avraham Tsameret and Victor Steinberg

Department of Physics of Complex Systems, The Weizmann Institute of Science, Rehovot 76100, Israel

We present experimental results on novel pattern states which were observed in the Couette-Taylor flow subjected to an axial flow, in a wide range of the control parameters. Propagating Taylor vortices (PTV's), stationary spirals (SSP's), and moving spirals (MS's) were found as a result of a different symmetry breaking. These modes exhibit different wave-number selection. Novel states originating from an interaction between these patterns were also found. A "mixed phase" of PTV's and SSP's was identified. A "mode-competition" state, in which the PTV's and MS's are alternated in the column, is also described. Finally, a "disordered-Taylor-vortices" state was observed and characterized.

I. INTRODUCTION

The superposition of the circular Couette flow and the Poiseuille shear flow in the Taylor system with an axial flow, as has previously been shown by Snyder [1], results in a rich phase diagram which exhibits several types of periodic structures. The through flow at a relatively small Reynolds number value (Re < 4) causes the Taylor vortices to drift downstream, and the flow takes the form of propagating Taylor vortices (PTV). Besides the PTV mode, which was studied in detail recently [2–5], the system also exhibits spiral modes which can be classified by the helicity and direction of propagation as was done by Bühler and Polifke [6].

A phase diagram which manifests instability modes of different symmetries, such as the PTV and spiral modes, may exhibit interesting nonlinear dynamics in the vicinity of points or lines which separate different instability regions. In such regions interactions between two or more instability modes are expected to be observed. The study of such interactions between modes is important because it can possibly shed light on pattern selection processes and on the scenario by which a macroscopic system becomes spatially and temporally disordered. We found that the Couette-Taylor system with a superimposed axial flow exhibits novel dynamical states which result from interactions between the PTV and two spiral modes. A wave number selection in these modes was also identified and studied.

II. CHARACTERIZATION OF THE SYSTEM AND EXPERIMENTAL APPARATUS

The system consists of the Taylor column and an axial flow modification. One control parameter of the system which governs the rotation is the Taylor number, defined as

$$T = \frac{4\eta^2 d^4}{1-\eta^2}\left[\frac{\Omega}{v}\right]^2 , \tag{1}$$

where $d = R_2 - R_1$. In the following we will use the reduced Taylor number (at $\epsilon \ll 1$)

$$\epsilon = \frac{1}{2}\left[\frac{T-T_0}{T_0}\right] = (\Omega - \Omega_0)/\Omega_0 ,$$

as the rotation control parameter, where Ω_0 is the critical rotation speed for the onset of vortices without through flow, corresponding to the Taylor number T_0. We use below the control parameter $\epsilon = (\Omega - \Omega_0)/\Omega_0$, up to $\epsilon \simeq 1$. Here R_1 and R_2 are the radii of the inner and outer cylinders, respectively, $\eta = R_1/R_2$, v is the kinematic viscosity, and Ω is the rotation speed. A second control parameter which determines the axial flow is the Reynolds number $Re = \bar{v}d/v$, where $\bar{v}$ is the averaged velocity of the axial flow.

Two columns were used in the experiments, with the aspect ratios $\Gamma = L/d = 54$ and 48 (L is the length of the working-fluid region), and radius ratios $\eta = 0.707$ and 0.77, respectively. The radii of the outer cylinders were $R_2 = 2.685$ and 4.100 cm, and the radii of the inner cylinders were $R_1 = 1.900$ and 3.150 cm, respectively. The column was installed horizontally and was modified by an axial flow arrangement. The axial flow was driven by gravity in a closed loop, with the use of a pump. In order to make the axial flow as uniform as possible in the azimuthal direction, the fluid passed an inlet chamber before entering the working region between the cylinders. The inlet chamber was constructed with flow directors and a stainless-steel net with 0.25×0.25 mm^2 mesh size. The net was used as nonrotational lateral boundaries at both sides of the column. The working fluid was a mixture of glycerol in water. Typically, the fluid had a dynamic viscosity of $v = 3.0$ cS, which corresponds to a mixture of 32.4% by volume of glycerol in water at 22 °C. The viscosity of the fluid was determined from tabulated data [7], and was checked by measurements with a commercial viscometer (HAAKE CV-100). The temperature of the fluid was maintained constant to a level of ±25 mK. The temperature stability was achieved by circulating water in a jacket around the column by the use of a commercial refrigerator-heater circulating system, and by stabilizing the room temperature to within ±1 °C. Before entering the column, the fluid passed through a copper

tube which was immersed in the circulator water basin, so that the axial flow was stabilized to the desired temperature at the inlet. 1% Kalliroscope solution [8] was used for flow visualization. The details of the apparatus are described elsewhere [3,5].

III. THE PHASE DIAGRAM

We present the phase diagram of our system (with $\eta = 0.707$), in Fig. 1, in the parameter space defined by ϵ and Re. For small through-flow velocities (Re < 4.5) the PTV mode is observed. The PTV are manifested first in the convectively unstable region (between the convective and absolute instability lines which are denoted by the dashed and solid lines in Fig. 1, respectively), and dominate at larger ϵ in the absolutely unstable region. Another region of the PTV is located for larger values of Re (Re $\gtrsim$ 8).

Beyond Re $\simeq$ 4.5 the flow is spiral-like, with a periodic pattern of a "stationary spirals" (SSP) mode. The SSP are initiated near the inlet boundary, and they are observed in a part of the column at Re $\gtrsim$ 2.5. They fill the entire column, however, at Re $\simeq$ 4.5. As ϵ increases, the SSP mode is stable for larger values of Re. Another spiral mode, which will be referred to as "moving spirals" (MS), also occurs in the system. This mode is characterized by spirals which propagate downstream. Both spiral modes (SSP and MS) are characterized by helicity $m = 1$. The MS mode is located in two separated regions in the phase diagram. In the first, the MS mode appears at the onset, for 5.26 < Re < 6.07, and it is stable along a narrow strip in Re as ϵ increases. The ratio between the phase

velocities of the MS in this region and the PTV was found to be 1.68. At $\epsilon = 0.65$ the MS lose stability to the disordered-Taylor-vortices (DTV) state which is described below. The other region of the MS is located at 0.60 < ϵ < 1.45 and Re > 12.5, between the PTV region at smaller ϵ, and regions which exhibit interaction between modes, at larger ϵ.

Besides the regions that are characterized by the existence of one flow pattern only, the system exhibits also novel phases which result from interaction between two modes, either between the PTV and the SSP modes, or between the PTV and the MS modes. The interaction between the PTV and the SSP is observed in a narrow strip along the right boundary line of the SSP region, for 0.275 < ϵ < 0.98. This interaction gives rise to a novel state, the "mixed phase" [see enlargement (1) on Fig. 1]. The mixed phase is characterized by a superposition of velocity fields in both space and time of an oscillatory (PTV) mode and a stationary (SSP) mode.

An interaction between the PTV mode and the MS mode is manifested by two new states. The first is coined the "mode-competition" state, and is located on the phase diagram at 1.45 < ϵ < 1.54 and 14.0 < Re < 15.3 [see enlargement (2) on Fig. 1]. In this region the PTV and the MS are alternated in the column in a nonperiodic fashion. The second state which results from the interaction between the PTV and MS is coined "disordered-Taylor-vortices" state. This state is characterized by PTV, which are interrupted randomly by MS. We note that the transitions between the various states did not show hysteresis.

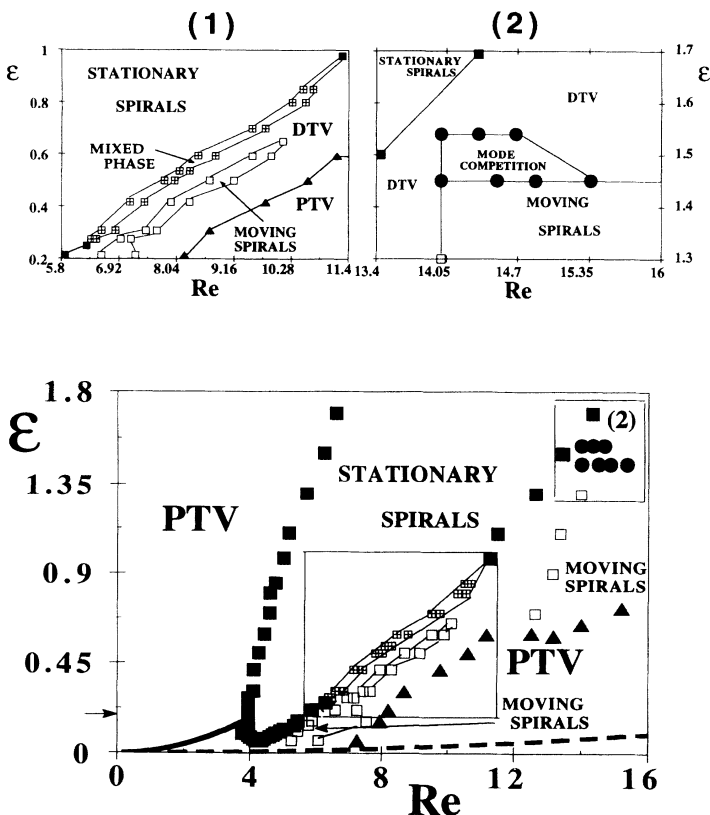The appearance of various periodic patterns with

FIG. 1. The phase diagram of the Taylor system with an axial flow, for $\eta = 0.707$. Three basic modes are observed: PTV, SSP, and MS. The regions in which the mixed-phase and the mode-competition state are manifested, are shown in the enlargement (1) and (2), respectively. DTV denotes the disordered-Taylor-vortices state. The arrow pointed to the ϵ axis denotes the line of constant $\epsilon = 0.19$, which corresponds to the plot of k vs Re presented in the next figure.

different symmetries in the system is related to a pattern selection process. One of the questions in this respect is whether the pattern formation is provided by a bulk property of the flow or by boundary effects, e.g., by a phase pinning. To answer this question we produced perturbations at the inlet boundary to cause an exchange of the SSP and the PTV modes. This experiment was carried out in the column with the radius ratio $\eta = 0.707$, for $5.8 < \text{Re} < 14$ and $\epsilon = 0.406$. The inlet boundary was designed as a moveable stainless mesh, whose motion is computer controlled. It was found that it is possible to change the flow pattern in the column from the SSP to the PTV by moving the inlet boundary on a distance of about 1 cm in the direction of the flow. The motion of the boundary generated a perturbation that induced the PTV, which took over the SSP in the system. A shorter traverse of the boundary was not enough to change the flow pattern. This procedure of changing the flow pattern from the SSP to the PTV was reproducible.

Changing the flow pattern from the PTV to the SSP was also found to be possible, however the perturbation that was required for this change was much larger. The induction of the stable SSP in the column was done by a fast pull of the inlet boundary for a distance of a few centimeters in the opposite direction of the flow. This perturbation was large enough to generate turbulent eddies near the inlet boundary. The procedure of changing the flow pattern from the PTV to the SSP was not easily reproducible, so that more than one perturbation was sometimes necessary in order to change the flow pattern. We note that by applying a quasistatical procedure, as was used in mapping the phase diagram, one obtains only one mode (PTV or SSP) for given control parameters, and there is a continuous transition between these modes. However, perturbations can excite the system to a metastable state (PTV in the region of SSP and vice versa), which probably have a finite (but long) life time.

We can conclude from the above observation that the pattern selection process in the system is possibly associated with a response to a perturbation in the boundary conditions.

Important information which is related to the phenomena of transitions between the various modes can be obtained from the measurements of the wave number of the various patterns, which we present further.

Wave-number selection

The wave-number measurements were carried out by taking pictures of the periodic patterns by a vidicon camera. The pictures were grabbed by an eight-bit frame grabber, and the wave number was calculated from the Fourier-transformed data.

We have found that the wave numbers of all the various periodic patterns were uniquely selected by the axial flow. The wave number was determined by the value of Re alone, and was insensitive to the specific procedure by which the pattern was set in the column, to the aspect ratio, or to the initial conditions. Such a wavelength selection was observed previously for the PTV mode in the small ϵ and small Re regime [2].

In Fig. 2 the wave number of the various periodic patterns vs Re is plotted for a constant $\epsilon \simeq 0.19$, for the column with $\eta = 0.707$. The solid circles correspond to the PTV in the small Re regime, the squares—to the SSP, the open circles— to the MS, and the triangles—to the PTV that appear at large Re. The states which result from an interaction between the basic modes were not presented in this figure. Figure 2 shows that the spiral modes and the large-Re PTV exhibit a decrease of the wave number with Re, which is approximately linear with Re. This behavior is in contrast to the wave-number behavior of the small-Re PTV, which exhibits an *increase* of k with Re; however, the variation of k does not exceed 10%.

Figure 2 demonstrates that the transition between the various modes in the system is associated with a jump in the wave number (except from the transition from PTV to SSP). A new flow pattern always appears after the wave number of the previous mode has reached a minimum. We observed that whenever the wave number of a certain mode is forced (by increasing Re) to reach its minimal value, the system does not allow an appearance of the same mode with a larger value of k, but rather generates a new mode. We note that in stationary states (such as stationary Taylor vortices [9]), whenever the vortices are forced beyond the Eckhaus boundary, the system responds with the same vortex pattern but with a wave number within the Eckhaus stable band.

The boundaries of the stable wave numbers for the spiral modes are shown in Fig. 3 as a function of ϵ. The solid squares and the open circles on the plot correspond to the SSP and the MS modes, respectively. The data points correspond to the extremal (maximal and minimal) values of k which are associated with the spiral modes. These points were obtained from measurements of k as a function of Re, similar to the measurement which is presented in Fig. 2. We note again that there is a one-to-one correspondence between a value of k within the band of the stable wave numbers, and Re value.

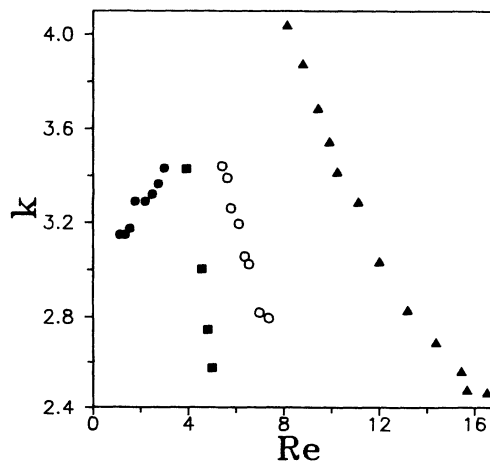FIG. 2. The wave number k vs Re, for PTV—solid circles, for SSP—solid squares, for MS—open circles, for large-Re PTV—triangles ($\epsilon \simeq 0.19$).
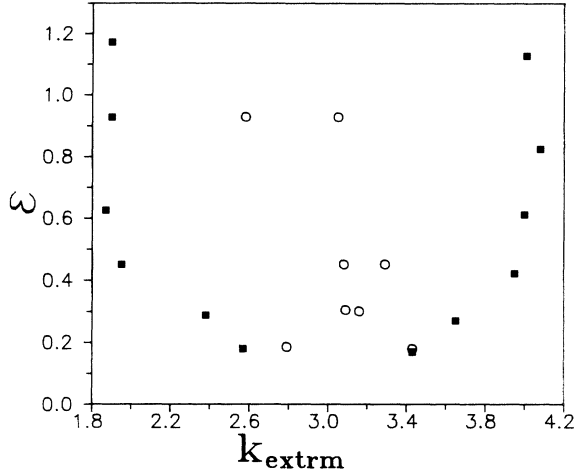
FIG. 3. The range of stable wave numbers vs ϵ for SSP (solid squares), and MS (open circles). The points correspond to the extrema of k vs Re curves.

IV. THE MIXED PHASE

The existence of a mixed phase, namely, a hydrodynamic state in which both stationary and oscillatory modes coexist in space and time, was predicted [10] by a theoretical analysis of the Rayleigh-Bénard convection in a viscoelastic fluid. The control parameters of this system are the temperature gradient and the elasticity of the fluid. The mixed phase was predicted to exist on the phase diagram of this system, in the vicinity of a codimension-two (CT) point [11] of the second type [10]. CT of the second type is characterized by the fact that the frequency of the oscillatory mode is finite as the CT point is approached. The interest in the mixed phase arose because the velocity field in this phase as predicted can exhibit a nonperiodic or incommensurate combination of the wave numbers of the two interacting modes. The study of the mixed phase could enrich our knowledge about interactions between hydrodynamic modes, and possibly the contribution of such interactions to the generation of complex pattern states.

The mixed phase which is found in our system is confined to a narrow region in Re (ΔRe$\simeq$0.2) along the right boundary of the SSP region on the phase diagram, in the range $0.275 < \epsilon < 0.98$. The mixed phase is located on the phase diagram between a region of the stationary SSP mode, and a region in which the flow pattern is chaotic (the DTV mode). As the mixed phase is approached from the SSP region, namely, as Re is increased at a constant ϵ, the stationary spiral pattern is modified by the PTV that appear at the inlet and propagate through the stationary spirals. The two modes coexist in the column. That is, at every point in space and time one can observe *both* modes.

The velocity field that corresponds to the flow pattern in the mixed phase is shown in Fig. 4, in which the intensity of the optical signal at successive time intervals is plotted as a function of position. The flow pattern is shown to be a superposition of a stationary and an oscillatory flow pattern. In this figure a space-time plot of the

full velocity field is shown in (a), alongside with a decomposition of the flow field to the oscillatory component (b), and the stationary component (c). The stationary component (c) was obtained by averaging the optical signal in time (over a time of typically $0.5\tau_v$). The oscillatory component was obtained by subtracting (c) from (a). It is seen that the amplitude of the oscillatory component is not spatially uniform, but is rather periodically modulated. The modulation, as will be shown shortly, results from a linear beating between two propagating modes, one of which is the PTV mode.

In order to clearly demonstrate that the flow in the mixed phase is indeed a superposition of stationary and oscillatory components, we have reproduced the velocity field in a computer simulation of the flow. The results of the simulation are presented in Fig. 5. The mixed phase flow is represented by the superposition of a stationary component and an oscillatory component, which itself is a superposition of two propagating modes. The stationary component, denoted by $S(x)$ and shown in Fig. 5(c), was extracted directly from the data, because the exact reproduction of this term by simulation is not simple and can unnecessarily complicate the picture. The oscillatory component, shown in Fig. 5(b), was represented by the term

$$A(x,t) = A_1(x,t) + A_2(x,t)$$
$$= a_1 \sin(k_1 x + \omega_1 t) + a_2 \sin(k_2 x + \omega_2 t) .$$

k_1 is the wave number of the PTV, as extracted from the data, thus, the term $A_1(x,t)$ represents the PTV mode. The term $A_2(x,t)$, which has a wave number $k_2 \simeq (\frac{1}{2})k_1$,
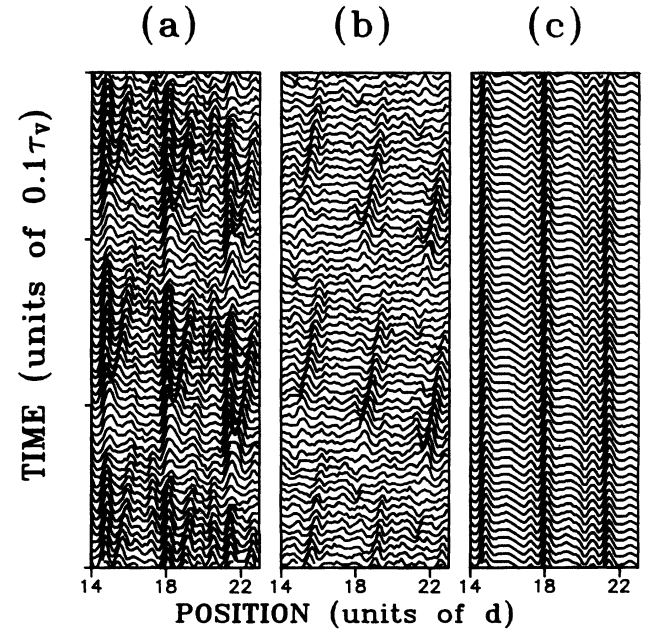

FIG. 4. A space-time plot for the velocity amplitude of the flow pattern in the mixed phase. The intensity of the optical signal is plotted as a function of the distance from the inlet at successive time intervals, for the full flow pattern (a), the oscillatory component (b), and the stationary component (c). Time goes up. (Re=7.5, ϵ=0.459.)
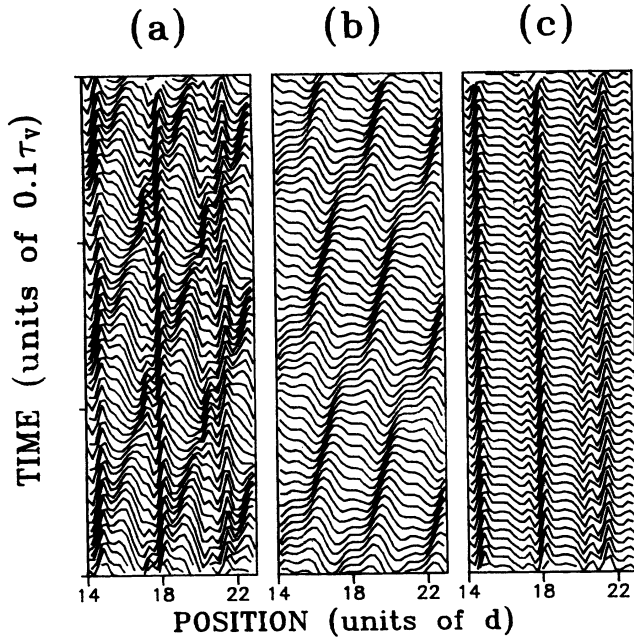
FIG. 5. Simulation of the velocity field in the mixed phase, for the full flow pattern (a), the oscillatory component (b), and the stationary component (c). See text for details.

probably results from the interaction between the PTV and SSP modes. The full superposed flow $aS(x) + A(x,t)$ is shown in Fig. 5(a). A good representation of the flow was found for $a_2 = 2a_1 = 5a$, $\omega_1 = \omega_2$, $k_1 = 3.74(1/d)$, and $k_2 = 1.74(1/d)$.

The amplitude of the oscillatory component in the mixed phase was found to exhibit an interesting spatial behavior. The velocity amplitude of the oscillatory component was found to vary spatially. Close to the inlet the amplitude always increases with the distance from the inlet, and farther away it may either increase, remain constant, or decrease with the distance from the inlet, depending on the values of the parameters ϵ and Re. An example is shown, in Fig. 6, which is a space-time plot of
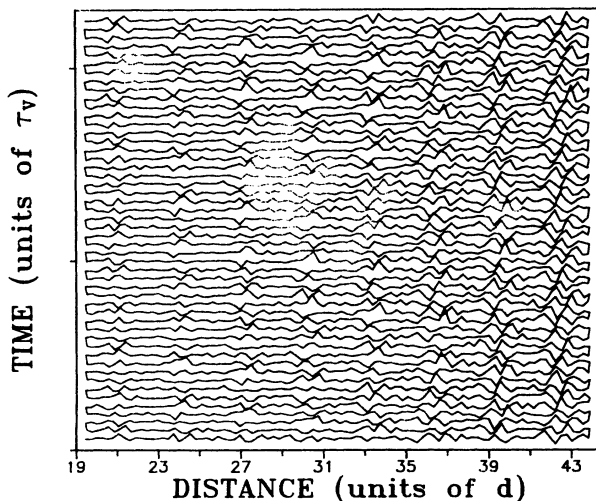

FIG. 6. A space-time plot of the oscillatory component of the flow pattern in the mixed phase, for Re=7.45, ϵ=0.417. Note the increase of the velocity amplitude with the distance from the inlet. Time goes up.
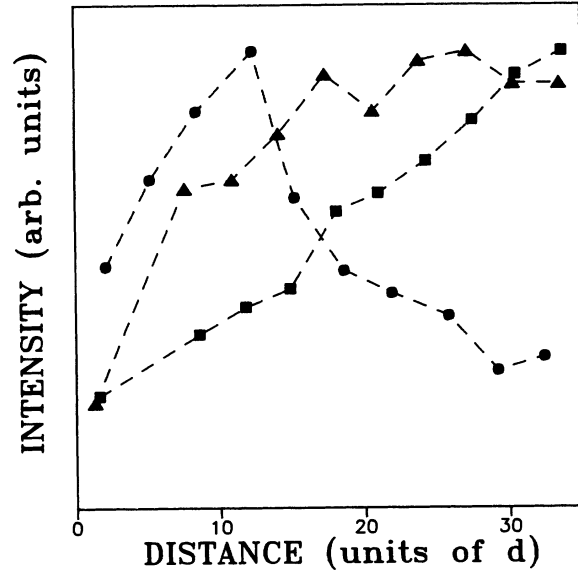

FIG. 7. The velocity amplitude in the mixed phase for several values of ϵ and Re: ϵ=0.275, Re =6.38 (squares); ϵ=0.50, Re =7.8 (triangles); ϵ=0.594, Re =8.45 (circles). The dashed lines are to guide the eye.

the oscillatory component for ϵ=0.417 and Re=7.45. This figure demonstrates an increase of the velocity amplitude with the distance from the inlet. This increase is characteristic for small ϵ, namely, $\epsilon < 0.5$. At $\epsilon \simeq 0.5$ the amplitude is roughly uniform far enough from the inlet, and for $\epsilon > 0.5$ the amplitude decreases with distance. The amplitude is shown, in Fig. 7, for three values of ϵ: the data for ϵ=0.275, 0.50, and 0.594; Re=6.38, 7.8, and 8.45 is presented by squares, triangles, and circles, respectively. The symbols on the plot correspond to local maxima of the velocity amplitude, and the lines are drawn only to guide the eye. The reason for the spatial variation of the amplitude is not clear, and a further study is required in order to understand this behavior.

The velocity field in the mixed phase that was observed in our system was shown to be relatively simple, namely, a linear superposition of the stationary and oscillatory modes. A more complicated flow pattern, that would possibly exhibit a chaotic behavior was predicted [10] to result from an interaction between two modes with incommensurate wavelengths.

V. MODE COMPETITION

In the "mode-competition" state two hydrodynamic modes compete for dominance in the system. This competition results in an alternation of the flow patterns associated with the competing modes.

A manifestation of mode competition in a different hydrodynamic system was found between transverse and longitudinal rolls in the Rayleigh-Bénard system with a binary mixture [12,13]. The competition between transverse and longitudinal rolls results in square cells, and leads to an oscillatory convection. A competition between transverse and longitudinal rolls, which lead to square cells with time-dependent amplitudes, was ob-

served also in a one-component Rayleigh-Bénard system subjected to a through flow [4]. In this system a region of irregular and intermittent flow pattern was observed. It was suggested that this pattern originated from the competition between the two types of rolls [14].

A mode-competition state is observed in our system in the region $1.45 < \epsilon < 1.54$ and $14.1 < Re < 15.3$. This state is characterized by an alternation between the PTV and the MS modes in the column. A pattern of either the PTV or the MS is present throughout the column for a certain period of time, and then disappears, and the other pattern becomes dominant. The mode-competition state differs from the mixed phase state by the fact that at the first state only one mode is present in the system at a given time.

The region of mode competition is found, quite surprisingly, between regions in the phase diagram in which the flow pattern is chaotic in space and in time—DTV, at $Re < Re_0 = 14.1$ and $Re > 15.3$. In the DTV, which will be described in the next section, the flow takes the form of the PTV which are randomly interrupted by the MS, so that no pattern dominates in the system at a given time. The existence of the state which exhibits order to some extent between the chaotic regions is reminiscent of locking regions in parametrically driven systems. More study is required in order to identify the mechanism behind the appearance of the mode-competition state in our system. In the following we present our observations of this state.

A typical space-time plot of the flow pattern in the mode-competition state is presented in Fig. 8, for $\epsilon = 1.45$ and $Re = 14.69$. The alternation between the two modes is clearly seen, because the phase velocity of the MS is larger than that of the PTV. The phase velocities of the two modes were determined from the space-time diagrams to be $V_p(\text{PTV}) = 1.66d/\tau_v$ and $V_p(\text{MS}) = 2.2d/\tau_v$.

The time during which each mode dominates in the system for a given Re and ϵ was not constant. Typical

FIG. 9. Typical histograms of the time durations of the PTV (a), and the MS (b) in the column ($\epsilon = 1.45$, Re = 14.69) in the "mode-competition" state.

histograms of the time durations of the two competing modes are presented in Fig. 9.

The averaged time duration in which one of the modes was present in the system was shown to vary with Re. At $Re \leq Re_0$ one observes that most of the time the MS are present in the system, and the PTV appear only seldomly and for a short time. PTV were observed for longer time periods for larger values of Re. The averaged time duration of the PTV increases with Re until a point where only the PTV were observed. Upon a further increase of
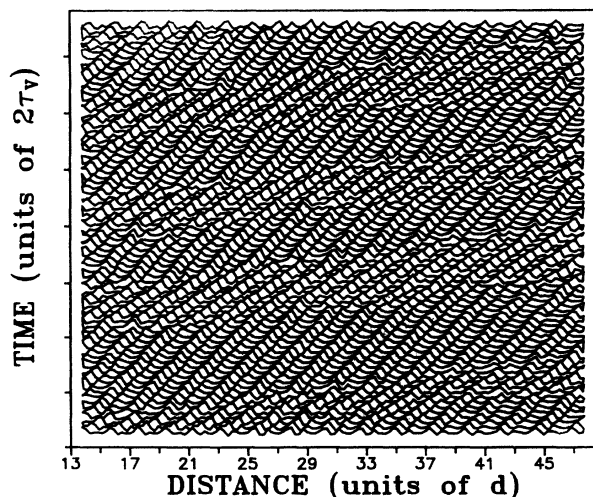
FIG. 8. A space-time plot of the flow pattern in the "mode-competition" state (Re = 7.45, $\epsilon = 0.417$). The MS can be distinguished from the PTV by their larger phase velocity. Time goes up.
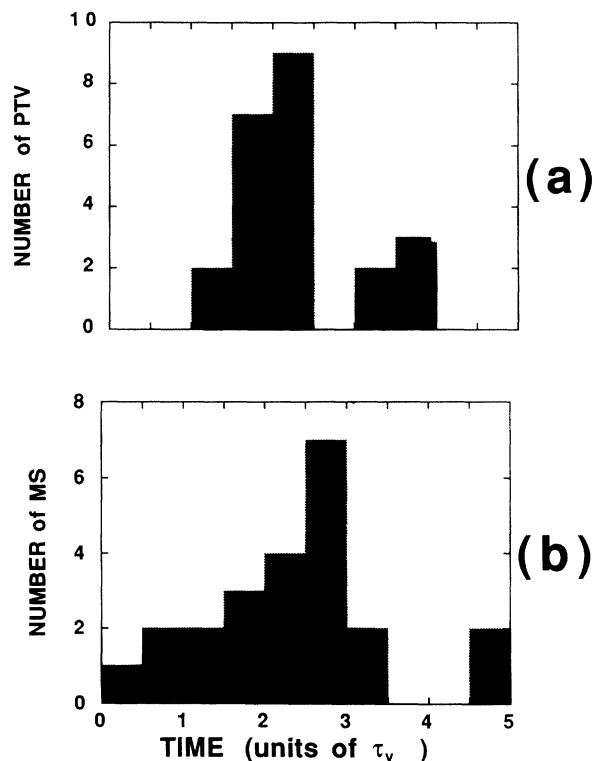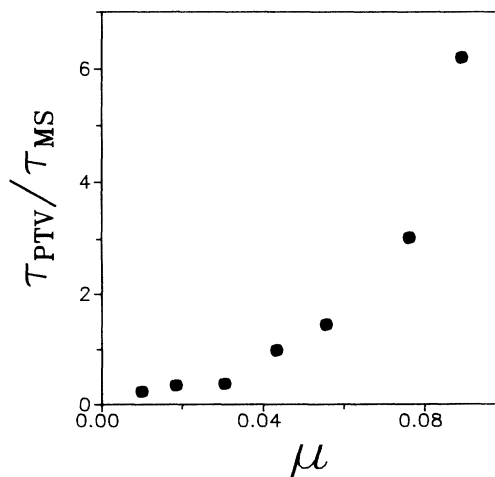
FIG. 10. The ratio between the averaged time durations of the PTV and the MS modes in the "mode-competition" state vs $\mu \equiv (Re - Re_0)/Re_0$ ($Re_0 = 14.1$).
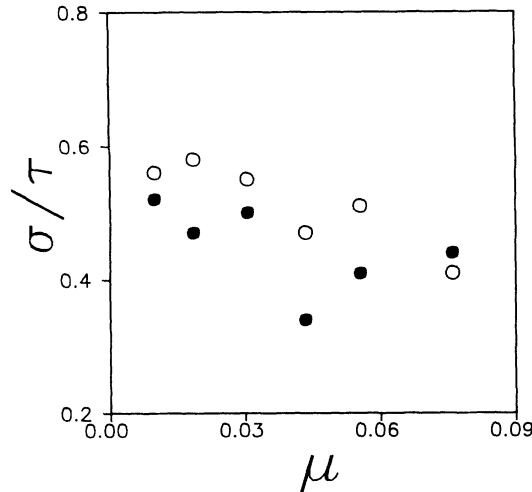
FIG. 11. The relative standard deviation of the time duration vs μ for the PTV (solid circles) and the MS (open circles).

FIG. 12. A space-time plot of the flow pattern in the DTV state, for $\epsilon=1.0$, Re $=12.24$. Note the pair of defects at the distance of about $12d$. Time goes up.

Re the PTV state was randomly perturbed by the MS, so that at a given time an ordered pattern could not be observed. A measurement of the relative time durations of the two modes was carried out, and the result is presented in Fig. 10. During the measurement time each pattern appeared in the column about 20 times. The x axis on the plot is $\mu=(Re-Re_0)/Re_0$, and the y axis is the ratio between the averaged PTV and MS time durations. The plot demonstrates the way by which the PTV mode takes over the MS mode as Re is increased.

The width of the distribution of the time duration of a pattern, either the PTV or the MS, was shown to increase or decrease with Re in the same way as that of the averaged time duration $\bar{\tau}$ of the pattern. In Fig. 11, the ratio of the variance $\sigma=\sqrt{1/N\sum_i^N(\tau_i-\bar{\tau})^2}$, and the averaged duration time $\bar{\tau}$, is shown as a function of μ, for the PTV mode (solid circles) and for the MS mode (open circles). It is seen from Fig. 11 that the normalized width of distribution is fairly constant with Re.

larger radius ratio, $\eta=R_1/R_2=0.77$. In spite of the relatively small change of η, the phase diagram of the system with $\eta=0.77$ did not exhibit an ordered pattern in the region Re >12, for $\epsilon\simeq1$. In this column the DTV state was found to be dominant in the range $12<$Re<22, which is much larger than in the column with $\eta=0.707$.

We present space-time plots of the DTV state in Figs. 12, 13, and 14, which show the intensity of the optical signal at successive time intervals taken by the vidicon camera. The plots correspond to $\epsilon=1.0$, and Re$=12.24$, 14.91, and 21.26, respectively. These plots demonstrate the breaking of the spatiotemporal order of the PTV mode by the MS. The effect of the MS is manifested by the appearance of spatiotemporal defects in the uniform spatiotemporal structure of the PTV. One pair of defects can be seen on the left-hand side of the space-time plot in Fig. 12, for example. For relatively small Re (Re$=12.24$), as is the case shown in Fig. 12, the defects are located mainly near the inlet boundary because most of the MS do not penetrate into the interior of the sys-

VI. THE DISORDERED-TAYLOR-VORTICES STATE

The DTV state is found on the phase diagram, presented in Fig. 1, in the transition region between regions which are dominated by either the PTV or the spiral modes. In the DTV state the PTV mode is perturbed randomly in time by the MS mode. The uniform spatiotemporal order, exhibited by the nonperturbed PTV mode, is broken by the MS, and the PTV mode becomes disordered. The degree of disorder depends on the rate of incidence of the MS in the system. It was found that the number of the MS that were initiated at the inlet boundary was increased with Re, but was independent of ϵ. Therefore, Re could be considered as a parameter that controls the degree of disorder exhibited by the DTV state. The DTV state may thus be an example for the study of the development of spatiotemporal chaos in an extended open system. It turned out that it is more convenient to conduct these studies in the column with a
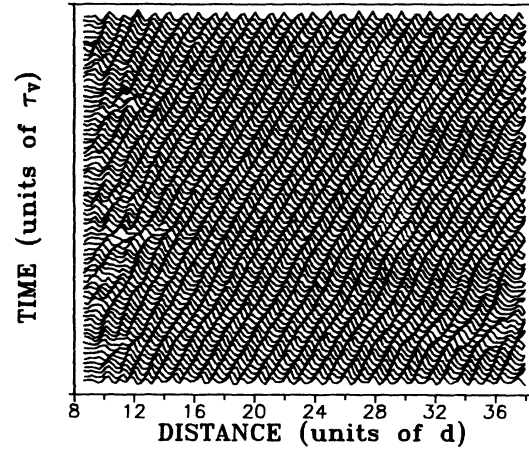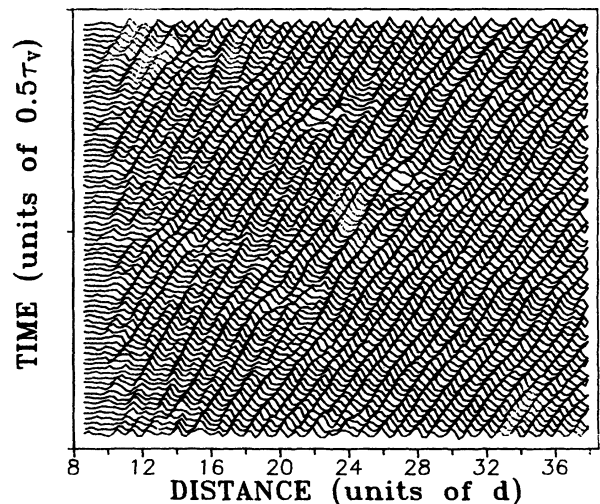

FIG. 13. A space-time plot of the flow pattern in the DTV state, for $\epsilon=1.0$, Re $=14.91$.
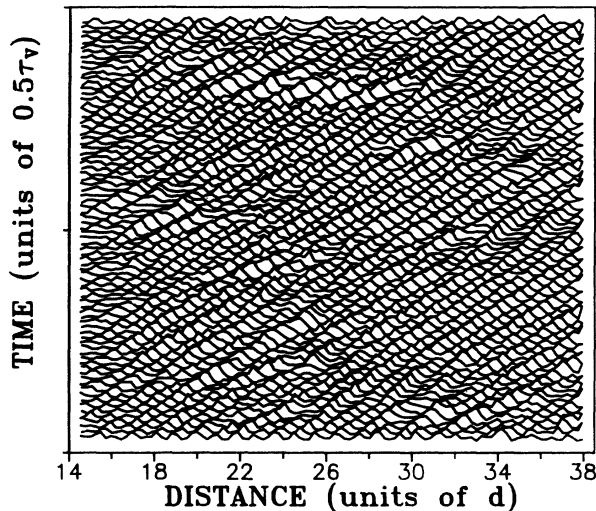
FIG. 14. A space-time plot of the flow pattern in the DTV state, for $\epsilon = 1.0$, Re $= 21.26$.

tem. Although defects are not observed near the outlet in Fig. 12, the MS still affect the PTV there by inducing a modulation of the phase velocity of the PTV, which is manifested as tilted PTV near the outlet. At larger Re, as in the case shown in Fig. 13 (Re$=14.91$), the MS penetrate into the interior of the system, and as a result the defects are found throughout the column. Finally, at still larger Re (Re$=21.26$ in Fig. 14) the pattern is strongly disordered everywhere.

A variety of nonequilibrium systems have revealed a state that can be defined as a spatiotemporal chaos [15–17]. In a part of these experiments an attempt to quantitatively characterize the order-disorder transition and the chaotic state has been made. A natural way to quantify the breaking of the long-range pattern coherency is to use a correlation function analysis. This approach was used successfully in two experimental systems [16,17] exhibiting a transition to defect-mediated turbulence. It allowed us to identify some features of the nonequilibrium order-disorder transition which are similar to an equilibrium phase transition. A destruction of spatiotemporal order may be associated with the appearance of spatiotemporal defects on space-time plots of the DTV. However, we would like to emphasize here that a $1+1$ representation of temporal dynamics of two-dimensional patterns definitely simplifies their analysis, but does not necessarily completely and adequately represent a complexity of their behavior. Since we did not perform a complete visualization of the column, we cannot be sure that there are no topological defects in the structure besides spatiotemporal dislocations. The existence of the former ones would obviously lead to an additional disorder in the system. Bearing in mind this consideration we characterized the degree of disorder of the DTV state as a function of the control parameter Re by two methods. First, we counted the number of defects as a function of Re in the corresponding space-time plots.

For each data set the data was divided into 12 space-time windows, each of which contained 80 lines separated by 200 msec in time (similar in size to the windows shown

in Figs. 12–14). The number of defects in each window was counted, and the mean number of defects and the standard deviation for the given data set was then calculated. We note that this analysis is similar to the analysis that was used in the study of the onset of spatiotemporal chaos in electroconvection of liquid crystals [16]. The onset of spatiotemporal chaos in electroconvection was found to be associated with the creation of topological defects in two-dimensional roll structure [16]. However, in the current analysis the second "dimension"—time, is arbitrary. Therefore, in order to compare the results for different Re values a time coordinate should be scaled by Re. As a result, the defect density $\bar{n}_d$ as a function of Re is presented in the inset of Fig. 15. One can associate an averaged distance between defects $\zeta \equiv \bar{n}_d^{-1/2}$ in the x-t plane with the coherence length of the DTV state. From the plot of ζ vs Re in Fig. 15 one can conclude that a sharp decline of the coherence length which is clearly evident at Re $\simeq 14$ and corresponds to a sharp increase in the averaged number of defects, indicates a destruction of the long-range order. This sharp change means a well-defined transition to an incoherent state with $\zeta \simeq (3-4)d$ at Re $\gtrsim 14$.

Another way to quantify the degree of disorder of the DTV state is to apply a correlation analysis. For a given value of Re the optical signal along the column was auto-correlated in space. The result was demodulated in order to obtain the envelope of the autocorrelated signal, and then was averaged in time (about 1000 lines, separated from each other by 200 msec, were used for time averaging). Figures 16–18 show the autocorrelated signal and the result of the averaging after demodulation, for three values of Re. As a result of the time averaging a spatial period-doubling modulation of the pattern becomes more pronounced. We did not identify the source of the modulation. The averaged signal was fitted by the function $F(x) = A + [B + C\cos(k/2)x]\exp(-x/l)$, and the correlation length l was obtained from the fit. The corre-
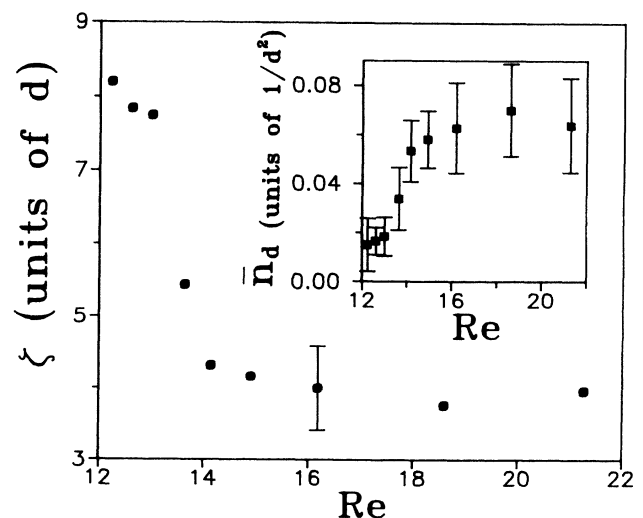

FIG. 15. The average distance between defects ζ vs Re in the DTV state. The inset: the defect density vs Re. The bars denote one standard deviation.
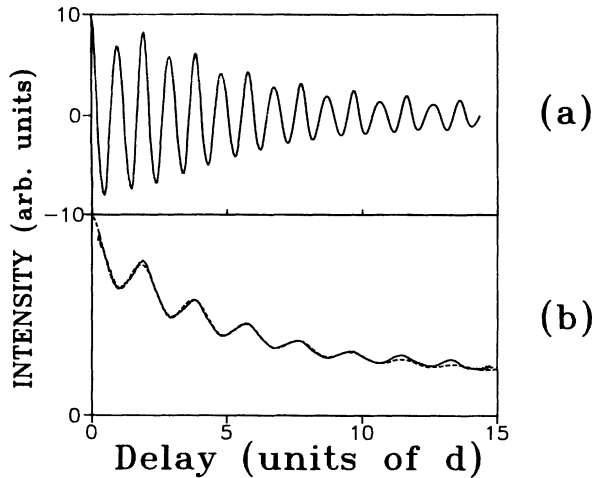
FIG. 16. (a) The spatial correlation function of the optical signal along the column. (b) Demodulated and time-averaged correlation function (solid line), and fit (dashed line). Re = 12.24, $\epsilon = 1.0$.
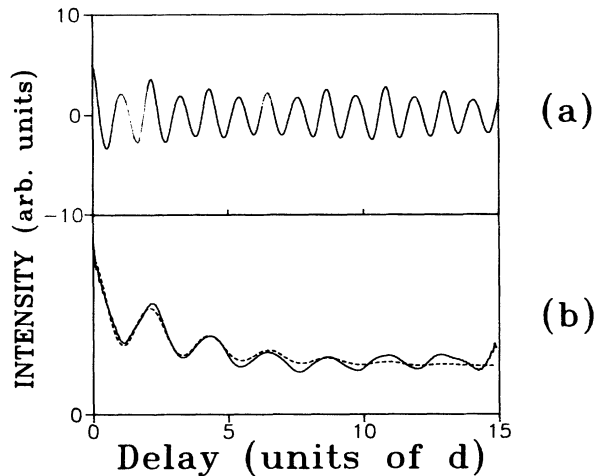
FIG. 19. The correlation length l, obtained from the fits to the time-averaged autocorrelated signals, vs Re in the DTV state.

FIG. 17. (a) and (b) the same as in Fig. 16 at Re = 13.0, $\epsilon = 1.0$.

sponding plot is shown in Fig. 19. The remarkable feature of the sharp drop of the correlation length down to the gap size at Re $\simeq 14$, similar to the sharp change of ζ given in Fig. 15, manifests the well-defined transition to the spatiotemporal disorder, where the long-range coherence of the structure is completely destroyed. We would like to point out a difference in the saturation values of ζ and l. It is feasible that the difference occurs due to the existence of an additional source of the disorder which is not captured, on the other hand, by a one-dimensional $(1 + 1)$ representation of the DTV state. Thus, the DTV state exhibits a spatiotemporal behavior similar to that found earlier in electroconvection of nematics [16] and in surface waves [17].

VII. SUMMARY

The phase diagram of the Couette-Taylor system with an axial flow in the range of Re < 22 and $\epsilon < 1.7$ was presented. Both stationary (SSP) and oscillatory (MS) spiral modes were observed, besides the PTV. The wave-number behavior of the various modes was discussed. It was found that the wave number of the spiral modes and of the large-Re PTV is decreased with Re, and that the transitions between the modes are associated with a jump in the wave number.

Novel states, which are originated from interaction between the PTV and spiral modes, were discovered. These states are as follows.

(i) The "mixed phase," in which both the oscillatory mode (PTV) and the stationary mode (SSP) coexist in space and time. The observed pattern in the mixed phase was shown to be reproduced in a computer simulation by a superposition of an oscillatory mode and a stationary mode.

(ii) The "mode-competition" state, in which the PTV and the MS are alternated in the column in an irregular fashion. This state, which exhibits a spatial order, is located between regions which exhibit a spatiotemporal dis-

FIG. 18. (a) and (b) the same as in Fig. 16 at Re = 21.3, $\epsilon = 1.0$. Note that (a) exhibits beats between two nearby wave numbers.

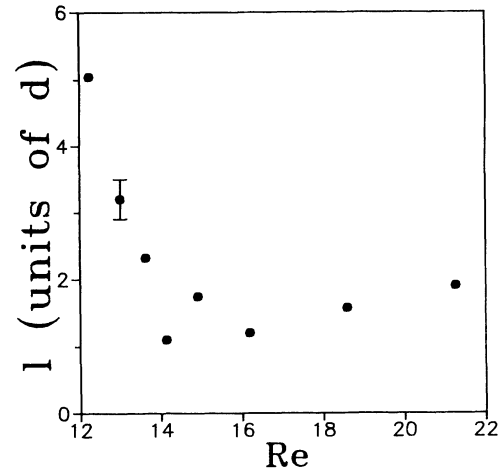order. Measurements and analysis of the duration times in which the two competing modes appear in the column were carried out.

(iii) The "disordered Taylor-vortices" state, in which the MS randomly perturb the PTV mode. The degree of disorder in the system, which is controlled by Re, was quantified by the analysis of the spatiotemporal defects in the structure, and by the correlation analysis.

[1] H. A. Snyder, Proc. R. Soc. London, Ser. A **265**, 198 (1962).

[2] A. Tsameret and V. Steinberg, Europhys. Lett. **14**, 331 (1991).

[3] A. Tsameret and V. Steinberg, Phys. Rev. Lett. **67**, 3392 (1991).

[4] K. L. Babcock, G. Ahlers, and D. S. Cannell, Phys. Rev. Lett. **67**, 3388 (1991).

[5] A. Tsameret and V. Steinberg, Phys. Rev. E **49**, 1291 (1994).

[6] K. Bühler and F. Polifke in *Non-linear Evolution of Spatio-temporal Structures in Dissipative Continuous Systems*, Vol. 225 of *NATO Advanced Study Institute, Series B: Physics*, edited by F. Busse and L. Kramer (Plenum, New York, 1990), p. 21.

[7] *CRC Handbook of Chemistry and Physics, D-235*, 65th ed. (CRC, Boca Raton, FL, 1984).

[8] Kalliroscope Co., P.O.B. 60, Groton, MA 01450, rheoscopic liquid AQ-1000.

[9] G. Ahlers, D. S. Cannell, M. A. Dominguez-Lerma, and R. Heinrichs, Physica D **23**, 202 (1986).

[10] B. J. A. Zielinska, D. Mukamel, and V. Steinberg, Phys. Rev. A **33**, 2 (1986).

[11] J. Guckenheimer and P. Holms, *Non-Linear Oscillations, Dynamical Systems and Bifurcations of Vector Fields* (Springer, New York, 1982), Chap. 7.

[12] E. Moses and V. Steinberg, Phys. Rev. Lett. **57**, 57 (1986).

[13] P. Le Gal, A Pocheau, and V. Croquette, Phys. Rev. Lett. **54**, 2501 (1985); P. Le Gal, Ph.D. thesis, Université de Paris–Sud, Centre d'Orsay, 1986 (unpublished).

[14] M. T. Ouazzani, J. K. Platten, and A. Mojtabi, Int. J. Heat Mass Transfer (UK) **33**, 1417 (1990).

[15] G. Ahlers, D. S. Cannell, and V. Steinberg, Phys. Rev. Lett. **54**, 1375 (1985); A. Pocheau, V. Croquette, and P. Le Gal, *ibid.* **55**, 1094 (1985).

[16] I. Rehberg, S. Rasenat, and V. Steinberg, Phys. Rev. Lett. **62**, 756 (1989).

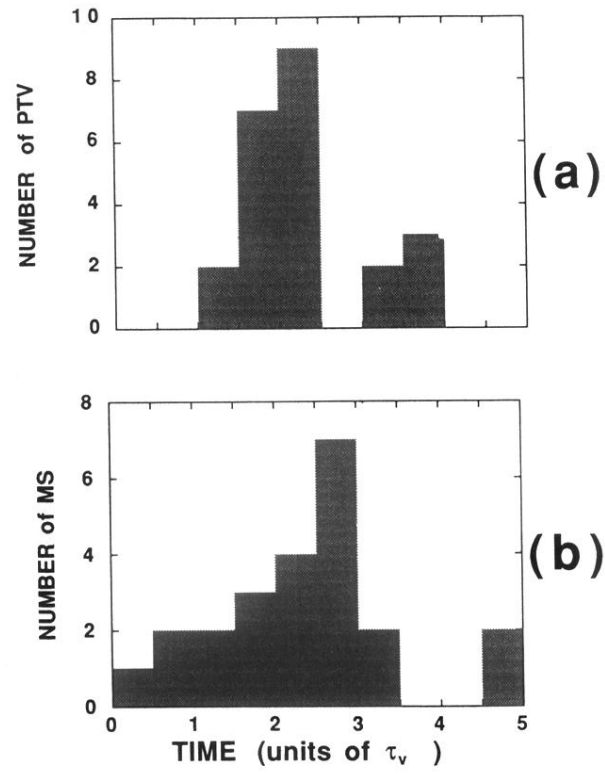[17] N. Tufillaro, R. Ramshankar, and J. Gollub, Phys. Rev. Lett. **62**, 422 (1989).

FIG. 9. Typical histograms of the time durations of the PTV (a), and the MS (b) in the column ($\epsilon = 1.45$, Re = 14.69) in the "mode-competition" state.